Heavy-strange meson decay constants in the continuum limit of quenched QCD

ALPHA
Collaboration

Michele Della Morte,[a] **Stephan Dürr,**[b] **Damiano Guazzini,**[c] **Rainer Sommer,**[c] **Jochen Heitger**[d] **and Andreas Jüttner**[ef]

[a] *CERN, Physics Department, TH Unit,*
 CH-1211 Geneva 23, Switzerland
[b] *Universität Bern, Institut für Theoretische Physik,*
 Sidlerstrasse 5, CH-3012 Bern, Switzerland
[c] *Deutsches Elektronen-Synchrotron DESY, Zeuthen,*
 Platanenallee 6, D-15738 Zeuthen, Germany
[d] *Westfälische Wilhelms-Universität Münster, Institut für Theoretische Physik,*
 Wilhelm-Klemm-Strasse 9, D-48149 Münster, Germany
[e] *University of Southampton, Department of Physics and Astronomy,*
 Highfield, Southampton SO17 1BJ, United Kingdom
[f] *Johannes Gutenberg-Universität Mainz, Institut für Kernphysik,*
 Johann-Joachim-Becher-Weg 45, D-55099 Mainz, Germany
 E-mail: `dellamor@mail.cern.ch`, `damiano.guazzini@desy.de`,
 `rainer.sommer@desy.de`, `heitger@uni-muenster.de`, `juettner@kph.uni-mainz.de`

Abstract: We improve a previous quenched result for heavy-light pseudoscalar meson decay constants with the light quark taken to be the strange quark. A finer lattice resolution ($a \approx 0.05$ fm) in the continuum limit extrapolation of the data computed in the static approximation is included. We also give further details concerning the techniques used in order to keep the statistical and systematic errors at large lattice sizes L/a under control. Our final result, obtained by combining these data with determinations of the decay constant for pseudoscalar mesons around the D_s, follows nicely the qualitative expectation of the $1/m$-expansion with a (relative) $1/m$-term of about $-0.5 \, \mathrm{GeV}/m_{\mathrm{PS}}$. At the physical b-quark mass we obtain $F_{B_s} = 193(7) \, \mathrm{MeV}$, where all errors apart from the quenched approximation are included.

Contents

1. Introduction

A big experimental progress is expected for the next years in flavour physics, mainly due to the new LHCb experiment [1] at CERN, CDF at Tevatron and the future super-B factories [2]. It will then be possible to determine with a precision of a few percent all entries of the CKM matrix, which describes flavour changing currents in the Standard Model. For this programme to be successful and to provide constraints on New Physics beyond the Standard Model, accurate theoretical predictions to be compared with the experimental results are extremely important.

Lattice QCD is the most appropriate tool for such computations, as they involve matrix elements of the operators in the Weak Effective Hamiltonian among hadronic states and they therefore require a non-perturbative approach.

Still, b-quarks on the lattice pose a two-scale problem: the lattice spacing a must be smaller than $1/m_{\text{b}}$ and the size L must be large enough such that the physics is not distorted by finite-size effects. Heavy Quark Effective Theory (HQET) on the lattice, as formulated by Eichten and Hill in refs. [3, 4], allows to circumvent the problem in a theoretically sound way. Formally, it consists in an expansion of the QCD action and correlation functions in inverse powers of the heavy quark mass.

Numerical applications have been plagued for a long time by the exponential growth of the noise-to-signal ratio in static-light correlation functions. This is due to the appearance of power divergences in the effective theory. Such divergences are non-universal, and we have given in [5] first evidences how the problem can be overcome by minimally modifying the Eichten-Hill discretization of the static action.

The result has been substantiated by successive studies [6 – 9] and also in the theory with $N_f = 2$ dynamical quarks [10]. Most of the cases dealt with the non-perturbative renormalization of static-light operators in a finite-volume scheme.

Here we show that also for physically large volumes fine lattice resolutions can be reached and precise results obtained. To emphasize the importance of such studies, we find that the result for F_{B_s} in the continuum limit changes by one standard deviation (7%) of the result quoted in ref. [5]. At the same time, of course, we reduce the systematic uncertainty owing to the extrapolation to zero lattice spacing.

The dependence of the decay constant on the heavy quark mass can very well be reconstructed by combining the continuum static result with continuum results at quark masses around the physical charm quark mass. The connection of the two different regimes is smooth, once the renormalization and matching of the static result is taken into account with sufficient precision.

The paper is organized as follows. In section 2 we describe the numerical setup used in the static approximation. Section 3 deals with the fitting procedure adopted to extract effective energies and matrix elements. Results in the static approximation are collected in section 4, while section 5 contains details about the simulations with relativistic quarks around the charm and our central results. Conclusions are drawn in section 6. The discussion of contaminations from excited states in static-light correlation functions is deferred to the appendix.

2. Heavy-light hadron physics in the static approximation

We consider a heavy-light meson system in the framework of quenched $O(a)$ improved lattice QCD with Schrödinger functional boundary conditions, where the heavy quark flavour is treated at the leading order of HQET, the static approximation. The basic setup of the computations presented here follows our earlier determinations of hadron properties by means of numerical simulations of the QCD Schrödinger functional in physically large volumes, see e.g. refs. [11 – 13] for studies in the strange and charm quark sectors and refs. [5 – 7, 10] for B-physics applications.

A particularly important technical ingredient of extracting B-meson masses and matrix elements from lattice HQET is the use of the alternative discretizations of the static theory, which were introduced in refs. [5, 6] to temper the well-known problem of exponential degradation of the signal-to-noise ratio encountered in static-light correlation functions when computed with the traditional Eichten-Hill [4] lattice action for the static quark.

Among the static quark actions S_h studied in detail in ref. [6], in the present work we restrict ourselves to the "HYP-action", which turns out to yield the largest gain (of more than one order of magnitude compared to Eichten-Hill at time separations of about

1.5 fm) in the signal-to-noise ratios of static-light correlation functions. This action is constructed from the Eichten-Hill action through replacing the temporal parallel transporters in the lattice derivative acting on the heavy quark field by the HYP-link that is obtained by a sensibly chosen smearing prescription for the gauge links located within the neighbouring hypercube [14]. Actually, in the context of static quarks, there are two favourable parameterizations of the HYP-link available (referred to as "HYP1" and "HYP2" in the following), with the second being even superior to the first. For more details the reader may consult ref. [6].[1]

2.1 Correlation functions and their quantum mechanical representation

Our starting point are B-meson correlation functions defined in the Schrödinger functional with a vanishing background gauge field [15]. Quarks with finite masses, also referred to as relativistic quarks, are labelled with an index "l", and the static ones with an index "h". The $O(a)$ improved axial vector current in static approximation is then defined as

$$(A_{\rm I}^{\rm stat})_0(x) = A_0^{\rm stat}(x) + a\, c_{\rm A}^{\rm stat} \delta A_0^{\rm stat}(x) \tag{2.1}$$

with the (bare) unimproved current

$$A_0^{\rm stat}(x) = \overline{\psi}_{\rm l}(x)\gamma_0\gamma_5\psi_{\rm h}(x) \tag{2.2}$$

and its $O(a)$ counterterm

$$\delta A_0^{\rm stat}(x) = \overline{\psi}_{\rm l}(x)\gamma_j\gamma_5\frac{1}{2}\left(\overleftarrow{\nabla}_j + \overleftarrow{\nabla}_j^*\right)\psi_{\rm h}(x) \tag{2.3}$$

multiplied by the improvement coefficient $c_{\rm A}^{\rm stat}$. In order to suppress contributions from excited B-meson states to the correlation functions of interest, we implement wave functions $\omega(\mathbf{x})$ at the boundaries of the Schrödinger functional such that an interpolating B-meson field is constructed in terms of the boundary quark fields $\zeta_{\rm l}$ and $\overline{\zeta}_{\rm h}$. In this way, the correlation function of the static axial current, $f_{\rm A}^{\rm stat}$, takes the form

$$f_{\rm A}^{\rm stat}(x_0,\omega_i) = -\frac{1}{2}\left\langle (A_{\rm I}^{\rm stat})_0(x)\,\mathcal{O}(\omega_i)\right\rangle, \quad \mathcal{O}(\omega) = \frac{a^6}{L^3}\sum_{\mathbf{y},\mathbf{z}}\overline{\zeta}_{\rm h}(\mathbf{y})\gamma_5\,\omega(\mathbf{y}-\mathbf{z})\,\zeta_{\rm l}(\mathbf{z}). \tag{2.4}$$

The boundary-to-boundary correlator $f_1^{\rm stat}$,

$$f_1^{\rm stat}(T,\omega_i,\omega_j) = -\frac{1}{2}\left\langle \mathcal{O}'(\omega_i)\,\mathcal{O}(\omega_j)\right\rangle, \quad \mathcal{O}'(\omega) = \frac{a^6}{L^3}\sum_{\mathbf{y},\mathbf{z}}\overline{\zeta}_{\rm l}'(\mathbf{y})\gamma_5\,\omega(\mathbf{y}-\mathbf{z})\,\zeta_{\rm h}'(\mathbf{z}), \tag{2.5}$$

serves to cancel the overlap of the (boundary) interpolating fields $\mathcal{O}(\omega_i)$ with the B-meson state, as made explicit in eqs. (2.10) – (2.12).

---

[1] As the static quark action HYP2 became available only at a final stage of this project, only the simulations at our finest lattice resolution ($\beta = 6.45$) were done for both HYP-actions, HYP1 and HYP2.

As for the choice of $\omega(\mathbf{x})$ itself, we follow [5] and opt for a set of four hydrogen-like, spatially periodic wave functions

$$\omega_i(\mathbf{x}) = \frac{1}{N_i} \sum_{\mathbf{n} \in \mathbb{Z}^3} \overline{\omega}_i \left(|\mathbf{x} - \mathbf{n}L| \right), \qquad i = 1, \ldots, 4,$$

$$\overline{\omega}_1(r) = r_0^{-3/2} \, \mathrm{e}^{-r/a_0}, \qquad\qquad \overline{\omega}_2(r) = r_0^{-3/2} \, \mathrm{e}^{-r/(2a_0)},$$

$$\overline{\omega}_3(r) = r_0^{-5/2} \, r \, \mathrm{e}^{-r/(2a_0)}, \qquad \overline{\omega}_4(\mathbf{x}) = L^{-3/2}, \qquad\qquad (2.6)$$

with $a_0 = 0.1863 r_0$, the hadronic radius $r_0 = 0.5$ fm [16] and the normalization factors N_i fixed by $a^3 \sum_{\mathbf{x}} \omega_i^2(\mathbf{x}) = 1$. Apart from investigating the Schrödinger functional correlators for single wave functions, it is now also possible (and — as will become clear in the next sections — even advantageous in practice) to form suitable linear combinations of two of them in order to cancel the first excited state in the B-meson channel almost completely.

For large T and x_0, the correlation functions $f_\mathrm{A}^\mathrm{stat}$ and f_1^stat allow for a computation of the pseudoscalar decay constant in the static approximation through the expression for the local renormalization group invariant (RGI) matrix element of the static axial current,

$$\Phi_\mathrm{RGI}^\mathrm{eff}(x_0, \omega_i) = -Z_\mathrm{RGI} \left(1 + b_\mathrm{A}^\mathrm{stat} a m_\mathrm{q} \right) 2 L^{3/2} \, \frac{f_\mathrm{A}^\mathrm{stat}(x_0, \omega_i)}{\sqrt{f_1^\mathrm{stat}(T, \omega_i, \omega_i)}} \, \mathrm{e}^{(x_0 - T/2) E_\mathrm{eff}(x_0, \omega_i)}, \qquad (2.7)$$

where the effective energy E_eff reads

$$E_\mathrm{eff}(x_0, \omega_i) = \frac{1}{2a} \ln \left[\frac{f_\mathrm{A}^\mathrm{stat}(x_0 - a, \omega_i)}{f_\mathrm{A}^\mathrm{stat}(x_0 + a, \omega_i)} \right]. \qquad (2.8)$$

The O(a) improvement coefficients $c_\mathrm{A}^\mathrm{stat}$ (cf. eq. (2.1)) and $b_\mathrm{A}^\mathrm{stat}$ depend on the discretization prescription of the static theory and have been perturbatively determined in ref. [6]. In eq. (2.7), Z_RGI is the renormalization factor that relates the bare matrix elements of A_0^stat to the RGI ones. It is non-perturbatively known from ref. [17] for the relevant range of bare couplings employed here and has a negligible uncertainty in comparison to the statistical error associated with the bare matrix element. As long as $0 \ll x_0 \ll T$, the local RGI matrix element is expected to exhibit a plateau, from which eventually the value of Φ_RGI to enter the formula

$$F_\mathrm{PS} \sqrt{m_\mathrm{PS}} = C_\mathrm{PS} \left(M/\Lambda_{\overline{\mathrm{MS}}} \right) \times \Phi_\mathrm{RGI} + \mathrm{O} \left(1/M \right) \qquad (2.9)$$

for the pseudoscalar decay constant, F_PS, can be extracted. In this equation, m_PS is the meson mass, and the conversion function C_PS [17, 18] translates the RGI matrix elements of the static effective theory to the corresponding QCD matrix elements at finite values of the heavy quark mass. It is parameterized in terms of the RGI mass of the heavy quark (M) and the QCD Λ-parameter in the $\overline{\mathrm{MS}}$ scheme ($\Lambda_{\overline{\mathrm{MS}}}$) [19].

Before coming to describe our analysis procedure for the computation of Φ_RGI and the static binding energy based on simulation results for the correlation functions in eqs. (2.4) and (2.5), let us have a look at the quantum mechanical representation of these correlators. First, we write down the expressions for $f_\mathrm{A}^\mathrm{stat}$ and f_1^stat for large values of x_0 and $T - x_0$,

while L remains arbitrary at this stage. We neglect terms of order $\exp\{-(T-x_0)\,m_{\mathrm{G}}\}$, where the energy difference $m_{\mathrm{G}} = E_1^{(0)} - E_0^{(0)}$ is the mass of the 0^{++} glueball. In this approximation we obtain the decompositions [11]

$$-2f_{\mathrm{A}}^{\mathrm{stat}}(x_0,\omega_i) \approx \sum_{k\geq 0} \beta_i^{(k)} \mathrm{e}^{-x_0 E_k}\,, \quad \beta_i^{(k)} = \gamma^{(k)}\alpha_i^{(k)}\,, \tag{2.10}$$

$$2f_1^{\mathrm{stat}}(T,\omega_i,\omega_j) \approx \sum_{k\geq 0} \alpha_i^{(k)}\alpha_j^{(k)} \mathrm{e}^{-T E_k}\,. \tag{2.11}$$

Here, the energy E_0 of the lowest state can be identified with the binding energy E_{stat} of the static-light system, while in addition we have introduced

$$\alpha_i^{(k)} = \frac{\langle k,\mathrm{PS}\,|\,\mathrm{i}_{\mathrm{PS}}(\omega_i)\,\rangle}{\langle 0,0\,|\,\mathrm{i}_0\,\rangle}\,, \quad \gamma^{(k)} = \langle 0,0\,|\,\mathbb{A}_0^{\mathrm{stat}}\,|\,k,\mathrm{PS}\,\rangle \tag{2.12}$$

in terms of the k-th excited static B-meson state, $|\,k,\mathrm{PS}\,\rangle$, the vacuum $|\,0,0\,\rangle$ and the boundary states [11] $|\,\mathrm{i}_{\mathrm{PS}}(\omega_i)\,\rangle$ and $|\,\mathrm{i}_0\,\rangle$, all in the finite-volume normalization $\langle\,\psi\,|\,\psi\,\rangle = 1$. The desired static-light matrix element, related to the decay constant according to eq. (2.9), is then encoded in $\gamma^{(0)}$, because we have

$$Z_{\mathrm{RGI}}\left(1 + b_{\mathrm{A}}^{\mathrm{stat}} am_{\mathrm{q}}\right)\sqrt{2}\,L^{3/2} \times \gamma^{(0)} \equiv Z_{\mathrm{RGI}}\left(1 + b_{\mathrm{A}}^{\mathrm{stat}} am_{\mathrm{q}}\right)\Phi_{\mathrm{bare}} = \Phi_{\mathrm{RGI}}\,. \tag{2.13}$$

From the above definitions of the correlators one infers that Φ_{RGI} is of mass dimension $3/2$; thus, $r_0^{3/2}\Phi_{\mathrm{RGI}}$ is dimensionless.

2.2 Observables

According to the foregoing discussion, the Schrödinger functional correlation functions in eqs. (2.4) and (2.5) obey the following asymptotic behaviour for large x_0:

$$-2f_{\mathrm{A}}^{\mathrm{stat}}(x_0,\omega_i) \overset{x_0\to\infty}{\sim} \beta_i^{(0)} \mathrm{e}^{-x_0 E_{\mathrm{stat}}} + \beta_i^{(1)} \mathrm{e}^{-x_0(E_{\mathrm{stat}}+\Delta^{\mathrm{stat}})}\,, \tag{2.14}$$

$$2f_1^{\mathrm{stat}}(T',\omega_i,\omega_j) \overset{T'\to\infty}{\sim} \alpha_i^{(0)}\alpha_j^{(0)} \mathrm{e}^{-T' E_{\mathrm{stat}}}\,, \tag{2.15}$$

where Δ^{stat} denotes the energy gap to the first excited state in the pseudoscalar channel. In (2.15) it is already assumed that, for our values of T', contributions to f_1^{stat} from excited states can be neglected — an assumption justified by a numerical analysis in appendix A. Above, we further exploit the freedom to choose a different time extent $T' \neq T$ for the calculation of f_1^{stat}; the reason of this choice will become clear in the next section. From the large-time asymptotics of $f_{\mathrm{A}}^{\mathrm{stat}}$ and f_1^{stat} one concludes that E_{stat} and Φ_{RGI} can be obtained from the associated asymptotic behaviour of $E_{\mathrm{eff}}(x_0,\omega_i)$ and $\Phi_{\mathrm{RGI}}^{\mathrm{eff}}(x_0,\omega_i)$ as

$$E_{\mathrm{eff}}(x_0,\omega_i) \overset{x_0\to\infty}{\sim} E_{\mathrm{stat}} + \frac{\beta_i^{(1)}}{\beta_i^{(0)}}\frac{\sinh\left(a\Delta^{\mathrm{stat}}\right)}{a}\mathrm{e}^{-x_0\Delta^{\mathrm{stat}}}\,, \tag{2.16}$$

$$\Phi_{\mathrm{RGI}}^{\mathrm{eff}}(x_0,\omega_i) \overset{x_0\to\infty}{\sim} \Phi_{\mathrm{RGI}}\left\{1 + \frac{\beta_i^{(1)}}{\beta_i^{(0)}}\mathrm{e}^{-x_0\Delta^{\mathrm{stat}}}\left[1 + \left(x_0 - \frac{T'}{2}\right)\frac{\sinh(a\Delta^{\mathrm{stat}})}{a}\right]\right\}\,. \tag{2.17}$$

set	β	a [fm]	L/a	T/a	T'/a	$\kappa_{\rm s}$	$\kappa_{\rm c}$
A , A$'$	6.0	0.093	16	24	20	0.133929	0.135196
B , B$'$	6.1	0.079	24	30	24	0.134439	0.135496
C , C$'$	6.2	0.068	24	36	30	0.134832	0.135795
D , D$'$	6.45	0.048	32	48	40	0.135098	0.135701

Table 1: Simulation parameters for the calculation of the static-light correlation functions. Unprimed (primed) data sets refer to volumes $V = L^3 \times T$ ($V = L^3 \times T'$), and the statistics varies between O(1000) measurements for set B$'$ and O($2500 - 5000$) measurements for the other sets. All simulations employed the static action HYP1, except for $\beta = 6.45$, where both versions, HYP1 and HYP2 were used. The global periodicity phase in spatial directions of the quark fields [20] is set to $\theta = 0$ in all cases.

2.3 Simulation details

The simulation parameters of our data sets are summarized in table 1. The corresponding quenched gauge field ensembles have been generated by a standard hybrid overrelaxation algorithm, where each iteration consists of one heatbath step followed by a few (in our case five) microcanonical reflection steps, and the sequential evaluations of the correlation functions were separated by at least $5 - 10$ iterations.

Thanks to the precise knowledge of the RGI strange quark mass in the quenched approximation, $M_{\rm s}$ [12], as well as the O(a) improved relation between the renormalized PCAC quark mass and the subtracted bare quark mass $am_{\rm q} = \frac{1}{2} \left(\kappa^{-1} - \kappa_{\rm c}^{-1} \right)$ for the relevant range of bare couplings $\beta = 6/g_0^2$ [21], the mass of the light flavour can be directly fixed to the strange quark mass by proper choices of the hopping parameter, $\kappa = \kappa_{\rm s}$, without any need for interpolations in the light quark mass. More concretely, our values for $\kappa_{\rm s}$ at each β were obtained by solving $M_{\rm s} = Z_{\rm M} Z \left(1 + b_{\rm m} \, am_{\rm q} \right) m_{\rm q}$ for κ, where $Z_{\rm M}$ is known from [19], Z and $b_{\rm m}$ from [21] and the critical hopping parameters from [12].

3. Analysis strategies for the static-light sector

In this section we describe the extraction of the matrix element of the static-light axial current and of the static binding energy from the correlation functions. We start with $E_{\rm stat}$ and display the effective energies for the data sets with $\beta = 6.45$ and all wave functions in figure 1.

Apart from analyzing the correlation functions and the observables deriving from them separately for each wave function, it is advantageous to construct linear combinations,

$$\omega_{ij} = \frac{1}{N_{ij}} \left(\omega_i + \rho_{ij} \, \omega_j \right) , \tag{3.1}$$

which enhance the quality and the extent of the plateau in the effective energy by (approximately) eliminating the contribution of the first excited state. Since
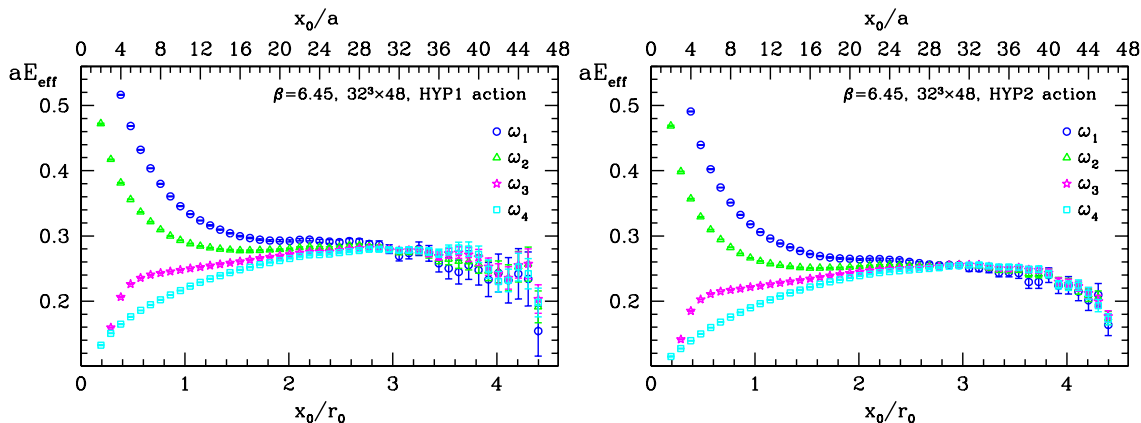
$$\rho_{ij} = -\beta_i^{(1)}/\beta_j^{(1)} \tag{3.2}$$

Figure 1: Effective static-light binding energy from data set D ($\beta = 6.45$, $32^3 \times 48$) for the static actions HYP1 (left) and HYP2 (right).

achieves this goal exactly, a practical way for finding such linear combinations is to perform a simultaneous fit to eq. (2.14) for all values of i, with $\beta_i^{(0)}$, $\beta_i^{(1)}$, E_{stat} and Δ^{stat} as fit parameters. Of course, the fit range has to be chosen with care. We list it together with the thus determined ρ_{ij} in table 2. Errors on the coefficients ρ_{ij} are shown for illustration, but we continue the analysis with just the central values. The so optimized correlation functions are subsequently analyzed without assuming anything on which excited state is present. In other words, we treat them just as if they were arbitrarily chosen trial wave functions. In the above analysis we excluded ω_3, since the time dependence of its effective energy, cf. figure 1, suggests that several states contribute in our chosen range for x_0. Still, we checked that upon including also ω_3 the final results of the next section are unchanged within their uncertainties.

After replacing the set of ω_i with the linear combinations ω_{ij}, the static binding energy E_{stat} is extracted by fits to eq. (2.16). Either this is done by dropping the correction term and fitting to a constant in a rather restricted interval, or we allow for smaller x_0 where deviations from a plateau are visible and include the correction term. These fits again may be performed simultaneously to all linear combinations with common fit parameters for the two energies. Obviously, having switched to the linear combinations of wave functions, the fit parameters in the correction term are expected to refer (approximately) to the second excited state. Indeed, for instance at $\beta = 6.45$, we now obtain a value of $a\Delta^{\text{stat}} \approx 0.60$, instead of $a\Delta^{\text{stat}} \approx 0.11$ for the original single wave functions with the HYP1 action.

As for the effective energy, also for the RGI matrix element of A_0^{stat} we have investigated several methods of computing this quantity from the static-light correlation functions at hand. For all lattices, and especially at higher β (and correspondingly larger T/a), we observe the dominant part of the statistical uncertainty of this quantity to be carried by the correlator between the Schrödinger functional boundaries, f_1^{stat}. Hence, as already anticipated in section 2.2, we have conducted additional simulations with temporal extensions $T' < T$, in order to reduce the error contribution to Φ_{RGI} from f_1^{stat} by calculating the latter on lattices with smaller time extents. Taking the crucial $\beta = 6.45$ data point as an

β	$S_{\rm h}$	(i,j)	$[\,t_{\rm min}/a, t_{\rm max}/a\,]$	ρ_{ij}
6.0	HYP1	$(1,2)$	$[10,18]$	$1.0(5)$
	HYP1	$(1,4)$	$[10,18]$	$0.23(5)$
	HYP1	$(2,4)$	$[10,18]$	$-0.21(5)$
6.1	HYP1	$(1,2)$	$[13,20]$	∞
	HYP1	$(1,4)$	$[13,20]$	$0.21(9)$
	HYP1	$(2,4)$	$[13,20]$	$-0.11(10)$
6.2	HYP1	$(1,2)$	$[13,24]$	$1.4(8)$
	HYP1	$(1,4)$	$[13,24]$	$0.23(6)$
	HYP1	$(2,4)$	$[13,24]$	$-0.16(6)$
6.45	HYP1	$(1,2)$	$[14,30]$	$1.1(6)$
	HYP1	$(1,4)$	$[14,30]$	$0.24(6)$
	HYP1	$(2,4)$	$[14,30]$	$-0.21(6)$
	HYP2	$(1,2)$	$[15,29]$	$1.5(7)$
	HYP2	$(1,4)$	$[15,29]$	$0.26(5)$
	HYP2	$(2,4)$	$[15,29]$	$-0.17(5)$

Table 2: Coefficients of the linear combinations for all data sets. The first linear combination for $\beta = 6.1$ coincides with the second wave function.

example, $f_{\rm A}^{\rm stat}(x_0, \omega_{ij})$ is computed on a $32^3 \times T/a$ lattice with $T = 48a$ and subsequently fitted to a two-state exponential ansatz as in eq. (2.14), i.e.

$$-2f_{\rm A}^{\rm stat}(x_0, \omega_{ij}) = \beta_{ij}^{(0)} {\rm e}^{-(x_0 - T'/2)E_{\rm stat}} + \beta_{ij}^{(1)} {\rm e}^{-(x_0 - T'/2)E_{\rm stat} - x_0 \Delta^{\rm stat}} , \qquad (3.3)$$

whereas $f_1^{\rm stat}$ originates from an *independent* evaluation of the data set generated in a simulation of a volume of $32^3 \times T'/a$, $T' = 40a$. The pairs (T, T') for the remaining values of β are included in table 1.

In the present situation, the RGI matrix element is given by eq. (2.13), where $\Phi_{\rm bare}$ is reconstructed as

$$\Phi_{\rm bare}(\omega_{ij}) = L^{3/2} \frac{\beta_{ij}^{(0)}}{\sqrt{f_1^{\rm stat}(T', \omega_{ij}, \omega_{ij})}} . \qquad (3.4)$$

While the non-linear fit parameters $E_{\rm stat}$ and $\Delta^{\rm stat}$ are constrained by simultaneous fits of $f_{\rm A}^{\rm stat}$ to eq. (3.3), the extracted $\Phi_{\rm bare}(\omega_{ij})$ are not constrained. We find them all nicely consistent. As an alternative, we also fit $\Phi_{\rm bare}^{\rm eff}(x_0, \omega_{ij}) = \Phi_{\rm bare}(\omega_{ij})$ in a restricted time interval and found entirely consistent values. We quote the latter as our central values.

4. Results in the static approximation

We follow the strategy explained in the previous section. An inspection of the plots for $E_{\rm eff}(x_0, \omega_{ij})$ is very useful to get a first impression of the quality and the extension of the plateaux as well as to select reasonable fit intervals for the numerical analysis.

Fits are performed in the range $t_{\rm min} \leq x_0 \leq t_{\rm max}$, where $t_{\rm max}$ is suggested by the x_0-dependence of $E_{\rm eff}(x_0, \omega_{ij})$ and, as already experienced in ref. [5], by the observation
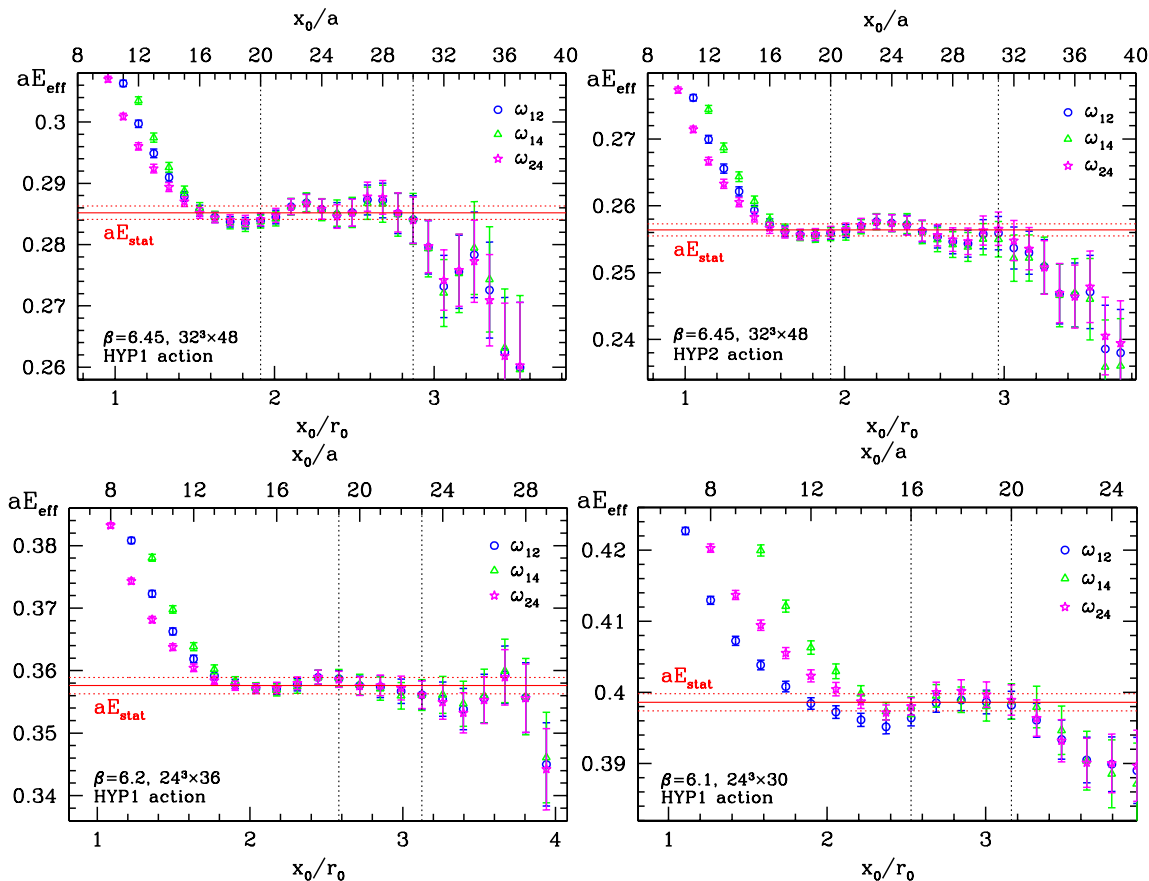
Figure 2: Top: Effective static-light binding energy from data set D ($\beta = 6.45$, $32^3 \times 48$) for the static actions HYP1 (left) and HYP2 (right) after construction of the linear combinations of wave functions, labelled ω_{12}, ω_{14} and ω_{24} in the panels. The final estimates of E_{stat} (obtained, as explained before, through fits within intervals given by the vertical dotted lines) are indicated by the horizontal lines, where the dashed lines show the error band. Bottom: Effective binding energies from data sets C (left) and B (right).

that an increase of $t_{\max}$ beyond a certain threshold (close to $3r_0$) is not convenient, because then the statistical uncertainties become too large. Sensible values for $t_{\min}$ may be inferred from the plots as well; we have kept them such that $t_{\min} > r_0 = 0.5$ fm [22] holds, while the stability of the fit parameters under shifts of $t_{\min} \to t_{\min} - r_0/2$ has always been checked. In particular, when dropping the excited state contribution, one has to take care of the fitting intervals to stay safely inside the plateau region of $E_{\text{eff}}(x_0, \omega_{ij})$. In these cases we usually had $t_{\min} \approx 2r_0$. Our results are collected in table 3. The final error for E_{stat} is the quadratic sum of the statistical error and the difference between the values for E_{stat} obtained by reducing $t_{\min}$ by $r_0/2$ with $t_{\max}$ being fixed.

The extraction of the static decay constant from the two different fits discussed in section 3 yields well compatible results. We list the ones from fits to a constant in table 3 and show them for $\beta = 6.1 - 6.45$ in figure 3. We checked the dependence of Φ_{RGI} upon the improvement coefficient $c_{\text{A}}^{\text{stat}}$ by setting the latter to its tree-level value and repeating the
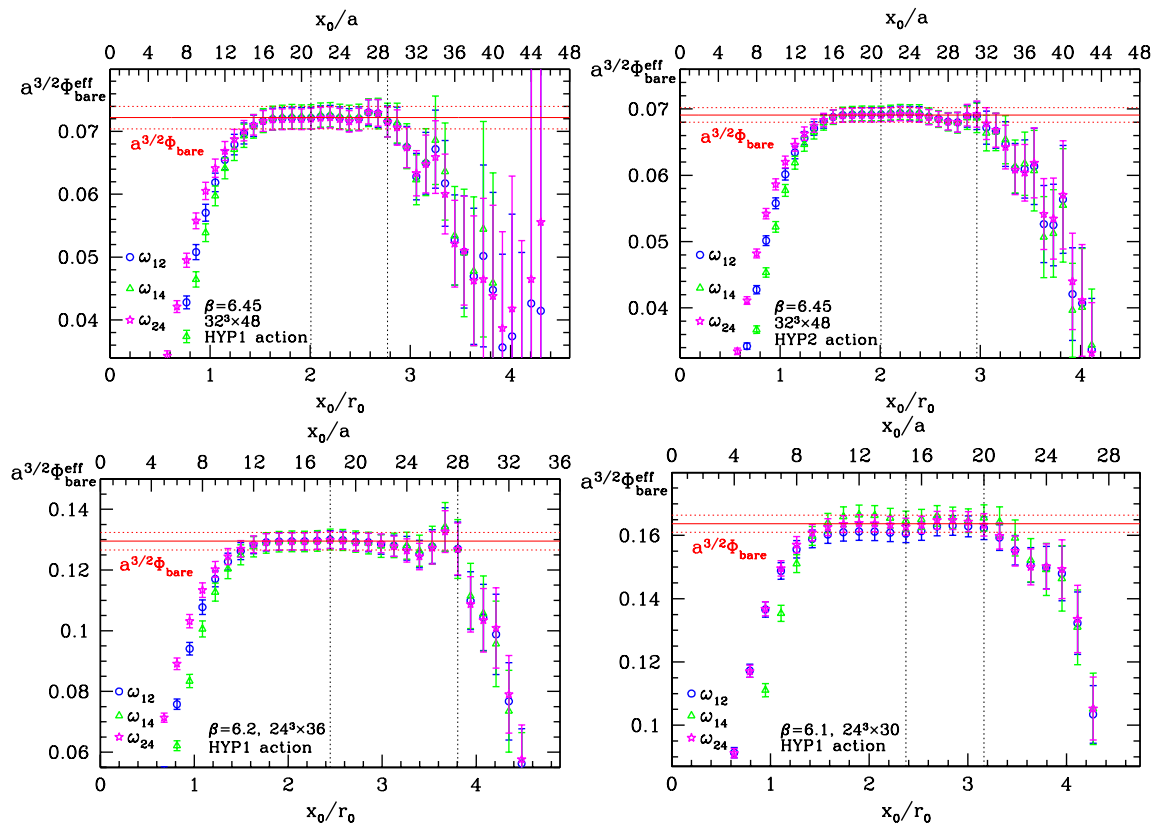
Figure 3: Top: Local matrix element of the static axial current from data set D ($\beta = 6.45$, $32^3 \times 48$) for the static actions HYP1 (left) and HYP2 (right) after construction of the linear combinations of wave functions, ω_{12}, ω_{14} and ω_{24}. The horizontal lines reflect the result for $a^{3/2}\Phi_{\text{bare}}$ and its error band (obtained through fits within intervals given by the vertical dotted lines). Bottom: Local matrix elements from data sets C (left) and B (right).

β	aE_{stat}	$a^{3/2}\Phi_{\text{bare}}(\omega_{ij})$	(i,j)
6.0	0.4363(13)	0.1976(19)	(2,4)
6.1	0.3986(12)	0.1637(27)	(2,4)
6.2	0.3576(13)	0.1295(29)	(1,2)
6.45	0.2852(11)	0.0722(18)	(1,2)
6.45*	0.2564(9)	0.0691(11)	(1,2)

Table 3: Results for the binding energy and the bare static-light decay constant. The entries in the last row refer to the HYP2 action.

whole analysis. The outcome of this exercise is again consistent with the numbers obtained before. One can thus conclude that the uncertainty in $c_{\text{A}}^{\text{stat}}$ does not affect our results and that they are expected to have all linear a-effects removed. For $\beta \leq 6.2$ and the HYP1 action there is full agreement with the results already published in ref. [5].

With the new data point at $\beta = 6.45$ a monotonic a-dependence is observed for $(a/r_0)^2 \leq 0.026$. Therefore, after attaching the necessary renormalization and improvement factors (cf. eqs. (2.13) and (3.4)), we perform the continuum extrapolation of the
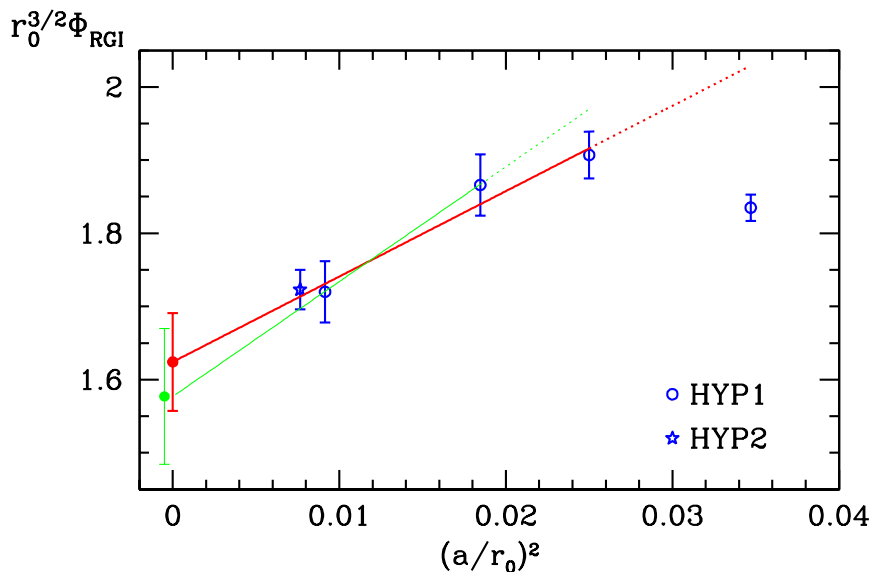
Figure 4: Three- and two-point continuum limit extrapolations of the RGI matrix element of the static axial current, represented by the red and the green line, respectively. The HYP2 result at $a \approx 0.05$ fm is not included in the extrapolation but only added for comparison. The continuum limit from the two-point fit and the HYP2 point are slightly moved to the left in the figure.

RGI matrix element of the static-light axial current (from the HYP1 data) within this range, see figure 4, and within a restricted range $(a/r_0)^2 \leq 0.019$, dropping the data point at $\beta = 6.1$ as well. In the continuum one finds $r_0^{3/2}\Phi_{\mathrm{RGI}} = 1.624(67)$ and $r_0^{3/2}\Phi_{\mathrm{RGI}} = 1.577(93)$ for the three- and two-point fit, respectively. As our final estimate we quote the result of the three-point extrapolation to ensure stability w.r.t. statistical fluctuations and supply it with the statistical error of the two-point fit as the total uncertainty to try to cover a systematic error due to possible higher-order terms in the a-expansion. This yields

$$r_0^{3/2}\,\Phi_{\mathrm{RGI}} = 1.624(93)\,, \tag{4.1}$$

which agrees within about one standard deviation with our results for both static actions at the smallest lattice spacing. Given the sizeable cutoff effects, it remains desirable to have results at an even finer lattice resolution to gain further confidence in the continuum extrapolation.

5. Decay constant at finite heavy quark mass

This section details how we compute the pseudoscalar decay constant in the continuum limit of large-volume quenched QCD with Schrödinger functional boundary conditions for pseudoscalar meson masses in the range $m_{\mathrm{PS}} = (1.5{-}2.6)\,\mathrm{GeV}$, composed of non-degenerate relativistic quarks. The heavy quark mass values thus cover a significant range around the physical charm region. Since it will turn out that the decay constant connects smoothly to the static result, Φ_{RGI}, the entire mass region $m_{\mathrm{PS}} \geq 1.5\,\mathrm{GeV}$ is covered and as an application, $F_{\mathrm{B_s}}$ can be extracted.

5.1 Relativistic correlation functions and observables

We compute the decay constant, defined through the QCD matrix element between a zero-momentum heavy-light pseudoscalar state and the vacuum, from the time component of the $\mathrm{O}(a)$ improved axial vector current on the lattice,

$$(A_\mathrm{I})_\mu(x) = A_\mu(x) + a\,c_\mathrm{A}\tilde{\partial}_\mu P(x)\,. \tag{5.1}$$

Here, $A_\mu(x)$ has the form given in eq. (2.2), section 2.1, with the static quark replaced by a heavy relativistic quark, and the improvement coefficient c_A in front of the symmetric lattice derivative $\tilde{\partial}_\mu$ acting on the pseudoscalar density $P(x)$ was non-perturbatively computed in [23].

$\mathrm{O}(a)$ improved correlation functions f_A and f_1 are defined just like $f_\mathrm{A}^\mathrm{stat}$ and f_1^stat, but only with the standard Schrödinger functional boundary sources ($\omega = \omega_4 = \mathrm{constant}$ in eq. (2.6)). Details are as in ref. [11]. For our choice of parameters, the effective mass derived from f_A exhibits a clear plateau already for these standard Schrödinger functional boundary sources so that in this part of our calculation we can pass on adjusting wave functions to improve the overlap with the ground state. Hence, we readily write down the expressions for the effective heavy-light pseudoscalar meson mass,

$$m_\mathrm{PS}(x_0) = \frac{1}{2a}\ln\left[\frac{f_\mathrm{A}(x_0 - a)}{f_\mathrm{A}(x_0 + a)}\right]\,, \tag{5.2}$$

and the corresponding effective pseudoscalar decay constant

$$F_\mathrm{PS}(x_0) = -Z_\mathrm{A}\left(1 + \tfrac{b_\mathrm{A}}{2}(am_{\mathrm{q},i} + am_{\mathrm{q},s})\right)\frac{2}{\sqrt{m_\mathrm{PS}L^3}}\frac{f_\mathrm{A}(x_0)}{\sqrt{f_1}}\,\mathrm{e}^{(x_0 - T/2)m_\mathrm{PS}}\,. \tag{5.3}$$

For large enough T and x_0 they equal the pseudoscalar mass and decay constant. Also the renormalization constant Z_A is non-perturbatively known [24], and $am_{\mathrm{q},i}$ and $am_{\mathrm{q},s}$ are the bare subtracted valence quark masses of the heavy and the strange quark, respectively. The coefficient b_A, non-perturbatively tuned in ref. [25], completes the $\mathrm{O}(a)$ improvement of our observables.

5.2 Simulation details

We have generated quenched gauge field ensembles for five different lattice spacings. The four coarser lattices have the same β-values as the ones summarized in table 1, section 2.3, and slightly different geometries $(L/a)^3 \times T/a = 16 \times 32$, 24×40, 24×48 and 32×64, respectively. In addition we have generated an ensemble with $(L/a)^3 \times T/a = 48^3 \times 96$ and $\beta = 6.7859$ which, using $r_0 = 0.5$ fm [16], corresponds to a lattice spacing of $a = 0.031$ fm [26]. As in the case of the simulations for the static-light observables, we employed a standard hybrid overrelaxation algorithm with 8 to 24 microcanonical reflection sweeps plus one heatbath sweep forming one iteration. Subsequent evaluations of the correlation functions were separated by 100 iterations for $\beta = 6.0$, 6.1, 6.2 and 6.45 and by 50 iterations for $\beta = 6.7859$. As before, we used the non-perturbatively improved Wilson quark action with c_sw taken from [23].

β	6.0	6.1	6.2	6.45	6.7859
n_{meas}	380	201	251	289	150
κ_1	0.134108	0.134548	0.134959	0.135124	0.134739
κ_2	0.128790	0.130750	0.131510	0.132690	0.132440
κ_3	0.123010	0.125870	0.127470	0.130030	0.130253
κ_4	0.119053	0.122490	0.124637	0.128131	0.128439
κ_5	0.115440	0.119370	0.122000	0.126330	0.126774
κ_6	0.112320	0.116640	0.119680	0.124730	0.123571
κ_7	0.109270	0.113960	0.117370	0.123120	0.117625

Table 4: Summary of simulation parameters for the calculation of heavy-light correlation functions with relativistic quarks. $\kappa_1 \equiv \kappa_{\mathrm{s}}$ corresponds to the bare subtracted valence quark mass of the strange quark, $am_{\mathrm{q,s}}$, while κ_i, $i = 2, \ldots, 7$, refer to our choices for the bare subtracted quark mass of the heavy flavour within the charm region.

In contrast to the hopping parameters in the static-light simulations described in section 2.3, we here have determined κ_{s} at each β by fixing the RGI strange quark mass to its value found at *finite lattice spacing* in [12].[2] Therefore, $\kappa_1 = \kappa_{\mathrm{s}}$ in table 4 differs from the choice in table 1 by $\mathrm{O}(a^3)$. The hopping parameter for the physical charm quark is known for the four coarser lattices [13], and through an extrapolation it was estimated at $\beta = 6.7859$. We then have guessed further hopping parameters in the vicinity of the charm quark value such as to yield a homogeneous covering of the region $m_{\mathrm{PS}} = (1.5 - 2.6)\,\mathrm{GeV}$ with simulation points.

5.3 Data analysis and results

Due to uncertainties in the determination of the simulation parameters, we do not obtain $F_{\mathrm{PS}}\sqrt{m_{\mathrm{PS}}}$ for each lattice spacing at exactly the same values of $r_0 m_{\mathrm{PS}}$. Therefore, we first interpolate it (at fixed lattice spacing) linearly in $1/(r_0 m_{\mathrm{PS}})$ to the common points $r_0 m_{\mathrm{PS}} = 3.768, 4.327, 4.955, 5.653, 6.211$ and 6.560, which are all close to the actual simulation points. In a second step we estimate the continuum limit of the decay constant, $r_0^{3/2} F_{\mathrm{PS}}\sqrt{m_{\mathrm{PS}}}$, at fixed $r_0 m_{\mathrm{PS}}$.

Since we expect $\mathrm{O}(a^2)$ scaling to break down for too large values of the heavy quark masses [28], we follow ref. [29] and exclude data points with $aM \gtrsim 0.64$ from the discussion of the continuum limit. Representative examples for the a-dependence are shown in figure 5. Since the slope of the data at small lattice spacings is not well determined, but on the other hand we have results very close to the continuum limit itself, we take as our central value for the continuum limit the (weighted) average of the data at the two smallest lattice spacings. To account for a possible systematic error, we then added the difference between the average and the datum at $(a/r_0)^2 = 0.018$ linearly to the statistical uncertainty of this fit to a constant.

---

[2]In order to determine the hopping parameter of the strange quark for the lattice with the finest resolution, we were required to extrapolate the values for the strange quark mass in [12] and the quark mass renormalization constant to $\beta = 6.7859$. Details can be found in [27].
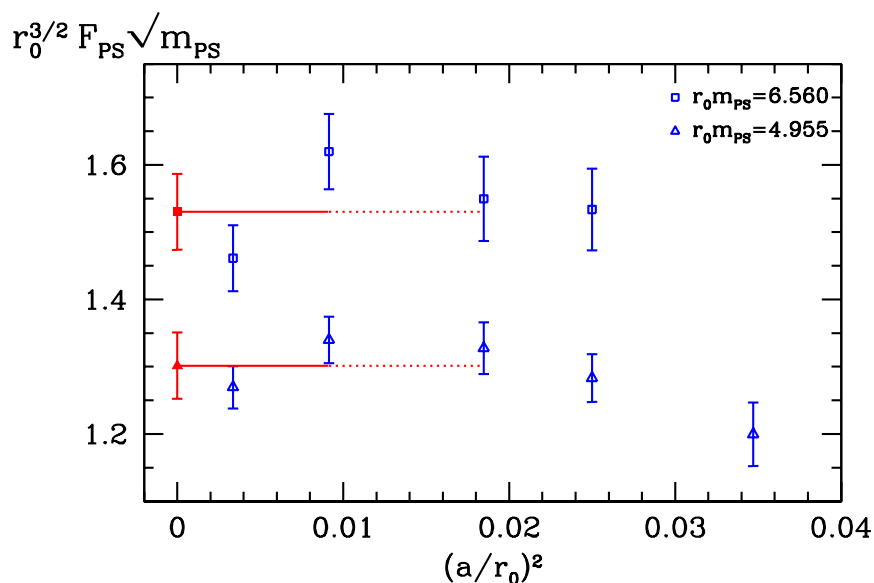
Figure 5: Lattice spacing dependence of the relativistic decay constants for two of the larger quark masses.
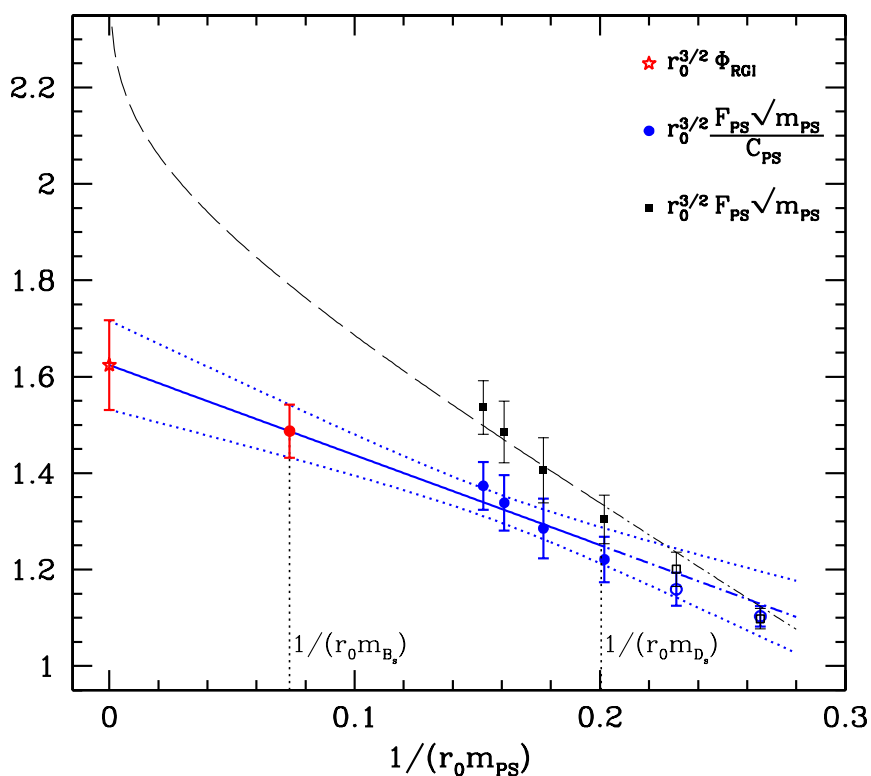

Figure 6: Interpolation of the decay constant between the result in the static limit (open red star) and the results in relativistic QCD (blue circles). The black squares do not include the matching coefficient $C_{\rm PS}$. Our final quenched result at the physical point of the $B_{\rm s}$-meson, $1/(r_0 m_{B_{\rm s}})$, is represented by the filled red circle: $r_0^{3/2} F_{B_{\rm s}} \sqrt{m_{B_{\rm s}}}/C_{\rm PS}(M_{\rm b}/\Lambda_{\overline{\rm MS}}) = 1.487(55)$.

The outcome of the continuum extrapolations of the relativistic decay constant for the available six values of the quark mass within the charm region is illustrated in figure 6. It nicely reflects that our continuum value for the RGI matrix element of the static-light axial current, given in eq. (4.1), can be perfectly combined with the associated QCD estimates by means of a linear interpolation down to even rather low values of the heavy-light meson mass of about $1.5\,\mathrm{GeV}$.

Indeed, as an effective description of the mass dependence of the decay constant, we fit the static result and the relativistic data points to the form suggested by the HQET expansion,

$$r_0^{3/2} \frac{F_{\mathrm{PS}}\sqrt{m_{\mathrm{PS}}}}{C_{\mathrm{PS}}\left(M/\Lambda_{\overline{\mathrm{MS}}}\right)} = A\left(1 + \frac{B}{r_0 m_{\mathrm{PS}}}\right)\,, \tag{5.4}$$

where we only include those points among the relativistic data into the fit that obey $m_{\mathrm{PS}} \gtrsim m_{\mathrm{D_s}}$ (cf. the filled blue circles in figure 6). Here, C_{PS} is the conversion function, which relates the static effective theory and QCD and has already appeared in (2.9). It is taken from perturbation theory in the form of [18]; its uncertainty is $\mathrm{O}\left(\alpha(m_{\mathrm{PS}})^3\right)$, estimated to be smaller than our statistical errors (see figure 2 in [18]). The resulting slope $B = -1.1(2)$ translates into

$$B/r_0 = -0.45(9)\,\mathrm{GeV} \quad \text{for} \quad r_0 = 0.5\,\mathrm{fm}\,. \tag{5.5}$$

We emphasize that eq. (5.4) and thus our value for the slope has to be considered an effective, phenomenological description and, consequently, B is an effective slope. A true HQET expansion can not be defined without a non-perturbative matching of the effective theory and QCD, i.e. a *non*-perturbative definition and estimate of C_{PS}. The reason is that at asymptotically large quark mass, any unknown perturbative correction in C_{PS} dominates over the non-perturbative $1/m$-term. We refer to ref. [30] for a more thorough explanation.

Converting the interpolation result $r_0^{3/2} F_{\mathrm{B_s}}\sqrt{m_{\mathrm{B_s}}}/C_{\mathrm{PS}}(M_{\mathrm{b}}/\Lambda_{\overline{\mathrm{MS}}}) = 1.487(55)$ to physical units (using $r_0\Lambda_{\overline{\mathrm{MS}}}$ from [19] and $r_0 M_{\mathrm{b}}$ from [7] in the evaluation of C_{PS} as well as the experimental $m_{\mathrm{B_s}}$-value) yields for the quenched decay constant of the $\mathrm{B_s}$-meson:

$$F_{\mathrm{B_s}} = 193(7)\,\mathrm{MeV}\,. \tag{5.6}$$

Being obtained from our effective description, this result is, however, *not* affected by our previous cautionary remarks on the HQET expansion. All that is needed for its determination is a safe interpolation, which eq. (5.4) does represent.

Finally, note that in an estimate of the $1/m_{\mathrm{PS}}$-correction the mass dependence in C_{PS}, i.e. the anomalous dimension of the current in the effective theory, plays a numerically important rôle. This is shown by the squares in figure 6 where, as an illustration, C_{PS} has been dropped. The difference reveals that C_{PS} accounts for about 50% of the mass dependence of $F_{\mathrm{PS}}\sqrt{m_{\mathrm{PS}}}$ in the considered region.

For other calculations of $F_{\mathrm{B_s}}$ we refer to [31–37] and references therein.

6. Conclusions

We have presented a computation of the heavy-light pseudoscalar meson decay constant in quenched lattice QCD reaching a precision in the continuum limit of around 4%. The

computation is founded on the O(a) improvement and non-perturbative renormalization of the relativistic theory and the static approximation of HQET carried out earlier by the ALPHA Collaboration. Here, we have added large-volume computations dealing with the heavy quark both in the static approximation and in relativistic QCD with masses around and somewhat heavier than the charm quark's mass.

The b-region is reached through a well controlled interpolation linear in the inverse of the meson mass. The final result for F_{B_s} is nicely consistent with refs. [38, 39], where different strategies are applied but the same inputs are used to fix the quenched theory.[3] The *effective* linear slope leads to a O($1/m_{PS}$) correction of about 10% at the physical b-quark mass. The effective linear pattern is preserved for masses in the charm region, and no evidence is found for O($1/m_{PS}^2$) corrections at the precision level of a few percents. These conclusions on the mass dependence of the decay constant depend on a precise enough knowledge of the conversion function C_{PS} [18] made possible through the perturbative result of ref. [40]. It will be very interesting to compare the present result with a direct HQET computation including $1/m$-corrections [41].

At the more technical level, an important rôle towards a sensitive reduction of the statistical uncertainty is played by the choice of two different physical time extents for the axial current correlator and for the boundary-to-boundary correlator in the effective theory, as well as in the construction of interpolating fields with wave functions. By exploiting the latter and the fitting methods used for the decay constant we also computed the binding energy of the static-light system for the HYP1 action in the range of couplings $6.0 \leq \beta \leq 6.45$ and at $\beta = 6.45$ for the HYP2 action. They are of interest in a computation of the b-quark mass [42, 7, 38, 39].

Acknowledgments

A. Ground state dominance for f_1^{stat}

In the description of the analysis method to extract Φ_{RGI} in section 3 we have implicitly assumed that eq. (2.15) holds and that contributions from the first and possibly higher excited states to f_1^{stat} in eq. (2.11) can be neglected.

In order to arrive at a quantitative criterion in how far this assumption is justified for our data, let us suppress the ω-dependence of the correlation functions to lighten the

---

[3]In order to determine the b-quark mass in [7], the spin-averaged B_s-mass was used instead of the pseudoscalar mass [38, 39], but this is a small effect of order $\Lambda_{QCD}^3/m_{B_s}^2$.

notation and write down the quantum mechanical representation of $f_1^{\rm stat}$ including the first excited state correction, taking over the notation introduced at the end of section 2.1:

$$2f_1^{\rm stat} = \left[\alpha^{(0)}\right]^2 {\rm e}^{-T'E_{\rm stat}} \left(1 + \left[\frac{\alpha^{(1)}}{\alpha^{(0)}}\right]^2 {\rm e}^{-T'\Delta^{\rm stat})}\right). \tag{A.1}$$

By virtue of eqs. (2.10) – (2.12), the coefficients $\alpha^{(k)}$ are related to the $\beta^{(k)}$ appearing in the corresponding decomposition of $f_{\rm A}^{\rm stat}$ through

$$\left[\frac{\beta^{(1)}}{\beta^{(0)}}\right]^2 = \left[\frac{\alpha^{(1)}}{\alpha^{(0)}}\right]^2 \left[\frac{\langle\, 0,0\,|\ \mathbb{A}_0^{\rm stat}\,|\,1,{\rm PS}\,\rangle}{\langle\, 0,0\,|\ \mathbb{A}_0^{\rm stat}\,|\,0,{\rm PS}\,\rangle}\right]^2 = \left[\frac{\alpha^{(1)}}{\alpha^{(0)}}\right]^2 \left[\frac{F_{\rm PS}^{{\rm stat},(1)}}{F_{\rm PS}^{\rm stat}}\right]^2, \tag{A.2}$$

where in the second step $\langle\, 0,0\,|\ \mathbb{A}_0^{\rm stat}\,|\,k,{\rm PS}\,\rangle \propto F_{\rm PS}^{{\rm stat},(k)}\sqrt{m_{\rm PS}}$ (with $F_{\rm PS}^{{\rm stat},(0)} = F_{\rm PS}^{\rm stat}$) has been used. Since we expect

$$\left[\frac{F_{\rm PS}^{{\rm stat},(1)}}{F_{\rm PS}^{\rm stat}}\right]^2 = {\rm O}(1), \tag{A.3}$$

we get $\left[\alpha^{(1)}/\alpha^{(0)}\right]^2 \sim \left[\beta^{(1)}/\beta^{(0)}\right]^2$, which leads to[4] the following correction term to $\Phi_{\rm RGI}$ owing to a second, higher state possibly present in $f_1^{\rm stat}$:

$$\Delta f_1 \approx \frac{1}{2}\left[\frac{\beta^{(1)}}{\beta^{(0)}}\right]^2 {\rm e}^{-T'\Delta^{\rm stat}}. \tag{A.4}$$

Here, $\beta^{(0)}$, $\beta^{(1)}$ and $\Delta^{\rm stat}$ are accessible through the two-state fits of $f_{\rm A}^{\rm stat}$ discussed in the main text.

After building linear combinations of the original wave functions, we find ${\rm e}^{-T'\Delta^{\rm stat}} = {\rm O}(10^{-6})$ so that the magnitude of Δf_1 is essentially driven by the ratio of the linear fit parameters $\beta^{(0)}$ and $\beta^{(1)}$. For all lattices and linear combinations we found Δf_1 to be orders of magnitude smaller than the statistical uncertainty associated with $\Phi_{\rm RGI}$ itself, thereby supporting the validity of the one-state dominance for $f_1^{\rm stat}$. As already pointed out in section 3, thanks to the construction of linear combinations we actually expect the estimated correction term to be predominantly governed by the second excited state instead of the first one that is written in the formulae of this appendix.

References

[1] LHCB collaboration, S. Barsuk, *The LHCb experiment: status and expected physics performance*, *Nucl. Phys.* **156** *(Proc. Suppl.)* (2006) 93.

[2] SuperKEKB Physics Working Group collaboration, A.G. Akeroyd et al., *Physics at super B factory*, hep-ex/0406071.

[3] E. Eichten, *Heavy quarks on the lattice*, *Nucl. Phys.* **4** *(Proc. Suppl.)* (1988) 170.

---

[4]Note that $f_1^{\rm stat}$ enters $\Phi_{\rm RGI}$ with a power of $-1/2$, cf. eq. (2.7).

[4] E. Eichten and B.R. Hill, *An effective field theory for the calculation of matrix elements involving heavy quarks*, *Phys. Lett.* **B 234** (1990) 511.

[5] ALPHA collaboration, M. Della Morte et al., *Lattice HQET with exponentially improved statistical precision*, *Phys. Lett.* **B 581** (2004) 93 [*Erratum ibid.* **B 612** (2005) 313] [`hep-lat/0307021`].

[6] M. Della Morte, A. Shindler and R. Sommer, *On lattice actions for static quarks*, *JHEP* **08** (2005) 051 [`hep-lat/0506008`].

[7] M. Della Morte, N. Garron, M. Papinutto and R. Sommer, *Heavy quark effective theory computation of the mass of the bottom quark*, *JHEP* **01** (2007) 007 [`hep-ph/0609294`].

[8] ALPHA collaboration, D. Guazzini, H.B. Meyer and R. Sommer, *Non-perturbative renormalization of the chromo-magnetic operator in heavy quark effective theory and the $B^* - B$ mass splitting*, *JHEP* **10** (2007) 081 [`arXiv:0705.1809`].

[9] F. Palombi, M. Papinutto, C. Pena and H. Wittig, *Non-perturbative renormalization of static-light four-fermion operators in quenched lattice QCD*, *JHEP* **09** (2007) 062 [`arXiv:0706.4153`].

[10] M. Della Morte, P. Fritzsch and J. Heitger, *Non-perturbative renormalization of the static axial current in two-flavour QCD*, *JHEP* **02** (2007) 079 [`hep-lat/0611036`].

[11] ALPHA collaboration, M. Guagnelli, J. Heitger, R. Sommer and H. Wittig, *Hadron masses and matrix elements from the QCD Schrödinger functional*, *Nucl. Phys.* **B 560** (1999) 465 [`hep-lat/9903040`].

[12] ALPHA collaboration, J. Garden, J. Heitger, R. Sommer and H. Wittig, *Precision computation of the strange quark's mass in quenched QCD*, *Nucl. Phys.* **B 571** (2000) 237 [`hep-lat/9906013`].

[13] ALPHA collaboration, J. Rolf and S. Sint, *A precise determination of the charm quark's mass in quenched QCD*, *JHEP* **12** (2002) 007 [`hep-ph/0209255`].

[14] A. Hasenfratz and F. Knechtli, *Flavor symmetry and the static potential with hypercubic blocking*, *Phys. Rev.* **D 64** (2001) 034504 [`hep-lat/0103029`].

[15] ALPHA collaboration, M. Kurth and R. Sommer, *Renormalization and O(a)-improvement of the static axial current*, *Nucl. Phys.* **B 597** (2001) 488 [`hep-lat/0007002`].

[16] R. Sommer, *A New way to set the energy scale in lattice gauge theories and its applications to the static force and α_s in* SU(2) *Yang-Mills theory*, *Nucl. Phys.* **B 411** (1994) 839 [`hep-lat/9310022`].

[17] ALPHA collaboration, J. Heitger, M. Kurth and R. Sommer, *Non-perturbative renormalization of the static axial current in quenched QCD*, *Nucl. Phys.* **B 669** (2003) 173 [`hep-lat/0302019`].

[18] ALPHA collaboration, J. Heitger, A. Jüttner, R. Sommer and J. Wennekers, *Non-perturbative tests of heavy quark effective theory*, *JHEP* **11** (2004) 048 [`hep-ph/0407227`].

[19] ALPHA collaboration, S. Capitani, M. Lüscher, R. Sommer and H. Wittig, *Non-perturbative quark mass renormalization in quenched lattice QCD*, *Nucl. Phys.* **B 544** (1999) 669 [`hep-lat/9810063`].

[20] S. Sint and R. Sommer, *The Running coupling from the QCD Schrödinger functional: a one-loop analysis*, *Nucl. Phys.* **B 465** (1996) 71 [`hep-lat/9508012`].

[21] ALPHA collaboration, M. Guagnelli et al., *Non-perturbative results for the coefficients b_m and $b_A - b_P$ in O(a) improved lattice QCD*, *Nucl. Phys.* **B 595** (2001) 44 [`hep-lat/0009021`].

[22] ALPHA collaboration, M. Guagnelli, R. Sommer and H. Wittig, *Precision computation of a low-energy reference scale in quenched lattice QCD*, *Nucl. Phys.* **B 535** (1998) 389 [`hep-lat/9806005`].

[23] M. Lüscher, S. Sint, R. Sommer, P. Weisz and U. Wolff, *Non-perturbative O(a) improvement of lattice QCD*, *Nucl. Phys.* **B 491** (1997) 323 [`hep-lat/9609035`].

[24] M. Lüscher, S. Sint, R. Sommer and H. Wittig, *Non-perturbative determination of the axial current normalization constant in O(a) improved lattice QCD*, *Nucl. Phys.* **B 491** (1997) 344 [`hep-lat/9611015`].

[25] T. Bhattacharya, R. Gupta, W.-j. Lee and S.R. Sharpe, *Scaling behavior of improvement and renormalization constants*, *Nucl. Phys.* **106** *(Proc. Suppl.)* (2002) 789 [`hep-lat/0111001`].

[26] S. Necco and R. Sommer, *The $N_f = 0$ heavy quark potential from short to intermediate distances*, *Nucl. Phys.* **B 622** (2002) 328 [`hep-lat/0108008`].

[27] A. Jüttner, *Precision lattice computations in the heavy quark sector*, `hep-lat/0503040`.

[28] ALPHA collaboration, M. Kurth and R. Sommer, *Heavy quark effective theory at one-loop order: an explicit example*, *Nucl. Phys.* **B 623** (2002) 271 [`hep-lat/0108018`].

[29] ALPHA collaboration, J. Heitger and J. Wennekers, *Effective heavy-light meson energies in small-volume quenched QCD*, *JHEP* **02** (2004) 064 [`hep-lat/0312016`].

[30] R. Sommer, *Non-perturbative QCD: renormalization, O(a)-improvement and matching to heavy quark effective theory*, `hep-lat/0611020`.

[31] CP-PACS collaboration, A. Ali Khan et al., *B meson decay constant from two-flavor lattice QCD with non-relativistic heavy quarks*, *Phys. Rev.* **D 64** (2001) 054504 [`hep-lat/0103020`].

[32] M. Wingate, C.T.H. Davies, A. Gray, G.P. Lepage and J. Shigemitsu, *The B_s and D_s decay constants in 3 flavor lattice QCD*, *Phys. Rev. Lett.* **92** (2004) 162001 [`hep-ph/0311130`].

[33] JLQCD collaboration, T. Onogi et al., *Heavy-light decay constants for B and D mesons in $N_f = 2$ unquenched QCD in Fermilab formalism*, *Nucl. Phys.* **129** *(Proc. Suppl.)* (2004) 373.

[34] UKQCD collaboration, C. McNeile and C. Michael, *Searching for chiral logs in the static-light decay constant*, *JHEP* **01** (2005) 011 [`hep-lat/0411014`].

[35] HPQCD collaboration, A. Gray et al., *The B meson decay constant from unquenched lattice QCD*, *Phys. Rev. Lett.* **95** (2005) 212001 [`hep-lat/0507015`].

[36] FERMILAB LATTICE AND MILC collaboration, C. Bernard et. al., *The decay constants f_B and f_D^+ from three-flavor lattice QCD*, `PoS(LAT2007)370`.

[37] A. Ali Khan et al., *Decay constants of charm and beauty pseudoscalar heavy-light mesons on fine lattices*, *Phys. Lett.* **B 652** (2007) 150 [`hep-lat/0701015`].

[38] D. Guazzini, R. Sommer and N. Tantalo, *m_b and f_{Bs} from a combination of HQET and QCD*, `PoS(LAT2006)084` [`hep-lat/0609065`].

[39] D. Guazzini, R. Sommer and N. Tantalo, *Precision for B-meson matrix elements*, *JHEP* **01** (2008) 076 [`arXiv:0710.2229`].

[40] K.G. Chetyrkin and A.G. Grozin, *Three-loop anomalous dimension of the heavy-light quark current in HQET*, *Nucl. Phys.* **B 666** (2003) 289 [`hep-ph/0303113`].

[41] B. Blossier, M. Della Morte, N. Garron and R. Sommer, *Heavy-light decay constant at the $1/m$ order of HQET*, `PoS(LAT2007)245` [`arXiv:0710.1553`].

[42] ALPHA collaboration, J. Heitger and R. Sommer, *Non-perturbative heavy quark effective theory*, *JHEP* **02** (2004) 022 [`hep-lat/0310035`].